Biomaterials Science

ROYAL SOCIETY OF CHEMISTRY

PAPER

View Article Online
View Journal | View Issue

Cite this: *Biomater. Sci.*, 2021, **9**, 4374

User-defined, temporal presentation of bioactive molecules on hydrogel substrates using supramolecular coiled coil complexes†

M. Gregory Grewal, [a] Vincent P. Gray, [a] Rachel A. Letteri [a] and Christopher B. Highley *[a,b]

The ability to spatiotemporally control the presentation of relevant biomolecules in synthetic culture systems has gained significant attention as researchers strive to recapitulate the endogenous extracellular matrix (ECM) *in vitro*. With the biochemical composition of the ECM constantly in flux, the development of platforms that allow for user-defined control of bioactivity is desired. Here, we reversibly conjugate bioactive molecules to hydrogel-based substrates through supramolecular coiled coil complexes that form between complementary peptides. Our system employs a thiolated peptide for tethering to hydrogel surfaces (T-peptide) through a spatially-controlled photomediated click reaction. The complementary association peptide (A-peptide), containing the bioactive domain, forms a heterodimeric coiled coil complex with the T-peptide. Addition of a disruptor peptide (D-peptide) engineered specifically to target the A-peptide outcompetes the T-peptide for binding, and removes the A-peptide and the attached bioactive motif from the scaffold. We use this platform to demonstrate spatiotemporal control of biomolecule presentation within hydrogel systems in a repeatable process that can be extended to adhesive motifs for cell culture. NIH 3T3 fibroblasts seeded on hyaluronic acid hydrogels and polyethylene glycol-based fibrous substrates supramolecularly functionalized with an RGD motif demonstrated significant cell spreading over their nonfunctionalized counterparts. Upon displacement of the RGD motif, fibroblasts occupied less area and clustured on the substrates. Taken together, this platform enables facile user-defined incorporation and removal of biomolecules in a repeatable process for controlled presentation of bioactivity in engineered culture systems.

Received 5th January 2021,
Accepted 28th April 2021

DOI: 10.1039/d1bm00016k

rsc.li/biomaterials-science

1. Introduction

The extracellular matrix (ECM) is intricate scaffolding that plays a central role in regulating cellular fates through multifaceted biophysical and biochemical processes.[1–4] In efforts to recapitulate microenvironmental features of the ECM *in vitro*,[5–7] the dynamic nature of the ECM must be considered, with the presentation of cell fate cues in flux during continual restructuring.[4,8–10] To develop culture systems that influence cell migration, proliferation, and differentiation, approaches are needed to engineer the presentation of molecules involved in cell fate decisions.[11–13] Hydrogel biomaterials are advantageous *in vitro* platforms as they can replicate tissue-specific mechanics and be modified with biomolecules through numerous established strategies.[14–17]

The immobilization of biomolecules onto or within tissue culture substrates is important when engineering environments that mimic the ECM.[18–21] One successful approach for incorporating bioactive molecules into scaffolds is photomediated thiol–ene click conjugation.[22–26] Modifying hydrogel-forming polymers with norbornene groups enables spatial control over biomolecule presentation *via* photo-mediated thiol–ene click conjugation when used in conjunction with photomasks that selectively shield light.[1,18,19,27] Controlling the localization of molecules on tissue culture scaffolds affords the ability to establish a spatial distribution of bioactive cues and gradients of signaling molecules to better recapitulate physiological environments and potentiate downstream cellular fates.[22]

While providing spatial control, a drawback of these covalent methods for conjugation of biomolecules to hydrogels is that the resulting materials do not capture the dynamic nature of *in vivo* cellular niches.[11,12,28,29] Cells continually transduce signals provided by biochemical and biophysical cues in their microenvironment,[30] and to achieve the dynamic characteristics of natural tissue in a biomaterial system, the

[a]*Department of Chemical Engineering, University of Virginia, VA 22903, USA. E-mail: highley@virginia.edu*
[b]*Department of Biomedical Engineering, University of Virginia, VA 22903, USA*
†Electronic supplementary information (ESI) available. See DOI: 10.1039/d1bm00016k

ability to define the presentation of relevant signals, both spatially and temporally, is necessary.[20] To this end, researchers have made significant strides developing techniques to dynamically introduce bioactive cues into hydrogel systems.[31,32] For example, photo-mediated thiol–ene conjugation with subsequent photocleavage by means of *o*-nitrobenzyl-based ether linkers enabled reversible incorporation of bioactive compounds into hydrogel networks.[11,28,33] Additionally, Grim *et al.* developed a method for repeatable biomolecule presentation *via* a reversible, light-mediated thiol–ene conjugation in conjunction with an engineered allyl-sulfide as a chain transfer agent.[12,29] In a biologically inspired example, 3,4-dihydroxy-L-phenylalanine (DOPA), a catechol-containing amino acid present in mussels, facilitated reversible incorporation of biomolecules through dynamic-covalent esters formed between DOPA and phenylboronic acid.[34] These methods demonstrate efficacy in reversible incorporation of biomolecules; however, they primarily leverage covalent bonds when immobilizing bioactive molecules – thus motivating exploration into reversibility driven by noncovalent interactions.

Supramolecular interactions offer approaches for dynamic incorporation of biomolecules into hydrogel scaffolds to capture the dynamic biochemical and biophysical features of cellular microenvironments.[35–39] For example, host–guest pairs within hydrogels rapidly assemble, but can dissociate under externally applied forces.[37,40,41] Boekhoven *et al.* achieved temporally controlled presentation of adhesive peptides within a hydrogel by appending the peptides to a naphthyl group for interaction with a β-cyclodextrin host immobilized to alginate.[41] Subsequent addition of a bio-inert peptide attached to a higher affinity adamantane guest displaced the adhesive peptide and resulted in smaller 3T3 fibroblast cell areas.[41] Additionally, oligonucleotides can be designed for reversible pairing through a process known as toehold-mediated strand displacement.[42–44] Two complementary oligonucleotides pair, with one of the oligonucleotides designed with a longer 'toehold' region that can remain unpaired prior to introduction of a third, longer oligonucleotide designed to be fully complementary with the toehold-containing sequence. Adding the longer complementary strand displaces the shorter oligonucleotide due to the higher affinity interaction between the two longer oligonucleotides. This non-covalent interaction facilitates reversible and repeatable addition of biomolecules under short timescales through differences in association affinities on hydrogel scaffolds.[42–44]

We sought here to adopt concepts from each platform to develop a new method that affords reversible, dynamic incorporation of bioactive molecules into hydrogel networks with spatiotemporal control. We employ coiled coil-forming peptides that supramolecularly assemble in a specific manner in solution.[45–47] Similar to toehold-mediated strand displacement with DNA, Gröger *et al.* showed coiled coil peptides can undergo a similar process.[45] Introduction of a longer, higher affinity peptide to a lower affinity, toehold-containing coiled coil complex (dissociation constant, $K_D \sim 10^{-8}$ M) displaced the shorter, lower affinity component and yielded a high affinity coiled coil ($K_D \sim 10^{-9}$ M).[45] These associations are similar in nature to other specific supramolecular assemblies, such as cyclodextrin-adamantane ($K_D \sim 10^{-5}$ M)[41] and cucurbituril host–guest systems ($K_D \sim 10^{-11}$–10^{-12} M).[36] We considered that the comparatively moderate affinities in the coiled coil system ($K_D \sim 10^{-8}$–10^{-9} M)[45] would allow for stable presentation of biomolecules over extended periods of time, with facile release potentiated *via* the addition of specific competitive molecules. Furthermore, while cyclodextrin and cucurbituril-based assemblies are reversible, the relatively straightforward synthesis and potential to reversibly trigger binding and release over multiple cycles under physiological conditions render coiled coil peptide platforms highly attractive for dynamic modulation of synthetic cellular microenvironments.

We hypothesized that coiled coil-forming peptides could be strategically designed to allow for both spatially-controlled conjugation *via* photo-mediated thiol–ene reactions and temporal control of biomolecule presentation *via* toehold-mediated strand displacement of coiled coil complexes. The ability to disrupt these associations and remove the biomolecules provides the desired constitutive "on/off" functionality – enabling facile reversible functionalization of *in vitro* culture systems. Herein, we describe the design, structural and thermodynamic characterization, and patterning of biomolecules using a coiled coil peptide-based system on both hyaluronic acid (HA) and fibrous polyethylene glycol (PEG) hydrogel surfaces. Using the patterned substrates, we demonstrate temporal attachment and release of biomolecules. To showcase the potential of this system in modulating bioactivity in engineered microenvironments, we build on previous work studying supramolecular assemblies in reversible modulation of cell adhesion and morphology *in vitro*.[41,43] The reversible presentation of an adhesive sequence enables visual confirmation of changes occurring at the cellular level of *in vitro* models and may be of use in studies perturbing microenvironmental adhesion to ECM-derived peptide binding sequences to understand cell fate decisions.

Taken together, this coiled coil-forming peptide system represents a compelling platform for reversible, spatiotemporally controlled presentation of bioactive molecules. We note that this user-defined release process can be repeated over multiple cycles, lending itself to applications that require spatiotemporally controlled presentation of biomolecules that can be modulated through external cues as well as be reloaded for subsequent multi-stage release. In addition to the examples discussed here, this platform may be broadly applicable to understanding and controlling biomolecular composition in cellular microenvironments, for example to dynamically present growth factors and cytokines to modulate bioactivity *in vitro*.

2. Materials and methods

2.1. Synthesis of norbornene-functionalized hyaluronic acid (NorHA)

NorHA was synthesized as previously described.[18] Briefly, sodium hyaluronate (HA, Lifecore, 62 kDa) was dissolved in de-

ionized (DI) water with Dowex 50 W × 8 ion-exchange resin (3 g resin per 1 g HA) for 2 h, and subsequently filtered, titrated to pH 7.02–7.05 with *tert*-butylammonium hydroxide (TBA, FisherSci) to yield HA-*tert*-butylammonium salt (HA-TBA). The final product was frozen at −80 °C, lyophilized, and stored under nitrogen. HA-TBA was then dissolved in anhydrous dimethyl sulfoxide (DMSO) and allowed to react with benzotriazole-1-yl-oxy-tris-(dimethylamino)-phosphonium hexafluorophosphate coupling reagent (BOP, Sigma, 0.3 mol equivalents relative to carboxylic acids on HA), and 5-norbornene-2-methylamine (nor-amine, Sigma, 1 mol equivalent relative to carboxylic acids on HA) to functionalize HA with norbornene groups. After ~2 h, the reaction was quenched with cold DI water, and the solution was transferred to a membrane (molecular weight cutoff: 6–8 kDa) and dialyzed against DI water for 5 d. Precipitate was removed by filtration, and the solution was re-dialyzed against DI water for 5 d prior to freezing at −80 °C, lyophilizing, purging with nitrogen, and storing at −20 °C until ready for use. The degree of modification was determined to be ~25% by ^{1}H nuclear magnetic resonance spectroscopy (^{1}H NMR, 500 MHz Varian Inova 500).

2.2. Peptide synthesis

All peptides used in this study, unless otherwise stated, were synthesized using a Liberty Blue (CEM) automated, microwave-assisted solid phase peptide synthesizer *via* Fmoc methods. Briefly, Rink amide resin (Advanced Chemtech, Rink Resin SS, 100–200 mesh, 1% DVB) was swollen with dimethylformamide (DMF, Aldrich, ACS reagent grade), and the immobilized Fmoc group removed with 20% (v/v) piperidine in dimethylformamide. Fmoc-protected amino acids (Advanced ChemTech, 0.2 M in DMF, 5 equivalents relative to theoretical available sites on the resin) and the coupling agents diisopropylcarbodiimide (DIC, Aldrich, 99%, 1 M in DMF) and Oxyma Pure (Advanced ChemTech, 1 M in DMF) were added to the reaction vessel and heated to 90 °C for 4 min. The Fmoc deprotection and coupling steps were repeated to build the peptide from the C-terminus to the N-terminus. For fluorescent peptides, 5(6)-carboxyfluorescein (Sigma Aldrich, ≥95%) was added last onto the N-terminus. The resultant peptides were cleaved from the resin with a cocktail of 92.5% trifluoroacetic acid (TFA, Aldrich, 99%), 2.5% triisopropylsilane (TIPS, Aldrich, 99%), 2.5% 2,2′-(ethylenedioxy) diethanethiol (DODT, Aldrich, 95%), and 2.5% DI water, and then isolated by precipitation into cold diethyl ether (Aldrich, ACS reagent, contains butylated hydroxytoluene as inhibitor) and centrifugation. After removal of ether under vacuum, the peptides were resuspended in DI water, frozen in liquid nitrogen, lyophilized, and stored at −20 °C as powders until ready for use. High performance liquid chromatography (HPLC) was used to determine peptide purity; since we noted no appreciable byproduct species, the peptides were used without further purification (Fig. S4†). Peptide primary structure was confirmed *via* electrospray ionization mass spectrometry (ESI MS, Fig. S2, 3 and Table S1†). Secondary structures were determined by circular dichroism (CD) spectroscopy (Fig. S5†).

2.3. Isothermal titration calorimetry

Experiments were performed using a standard volume affinity isothermal titration calorimeter (TA Instruments, New Castle, DE) with peptide solutions prepared in either 1× phosphate buffered saline (PBS) or NIH 3T3 fibroblast culture medium at indicated concentrations. Peptide solutions were adjusted to pH 7.4 using NaOH or HCl and then degassed for 10 min at 25 °C. Titrations consisted of an initial 2 μL injection, followed by 24 or 49 injections (10 μL each) of one peptide solution (150–200 μM) into 1.3 mL of a second peptide solution (10–20 μM). Following an initial delay of 200 s, injections were separated by 200 s. Experiments were performed at 25 °C with the stirring speed set to 125 rpm and the cooling rate set to medium. The reference cell was filled with 1.3 mL of degassed, deionized water. The thermograms were analyzed using NanoAnalyze software (TA Instruments) and heats of binding (in kJ mol^{-1}) were obtained by integrating the area under each injection peak in the baseline-subtracted thermograms, then dividing by moles of each injected volume. When possible, the resultant curves were then fit to either the independent (one site) or multiple sites binding models to obtain K_D values. Heats of dilution from blank injections – either peptide (150–200 μM) into 1× PBS/fibroblast medium or 1× PBS/fibroblast medium into peptide (10–20 μM) – were subtracted from experimental heats to yield the blank-corrected data.[48] In all analyses, we neglected the heats from the initial 2 μL injection.

2.4. Fabrication of NorHA hydrogels

Prior to formation of NorHA hydrogels, glass coverslips (22 × 22 mm) were functionalized with 3-(mercaptopropyl) trimethoxysilane (MTS, Sigma Aldrich, 95%) to present pendant sulfhydryl groups as follows. Briefly, glass coverslips were plasma treated (Harrick Plasma) for 3 min, and MTS was added dropwise to plasma treated surface prior to being baked at 100 °C for 1 h, and 120 °C for 10 min in an exhausted oven. The coverslips were washed sequentially in dichloromethane (DCM), 70% ethanol in water, and DI water, then stored under inert atmosphere until ready for use. NorHA hydrogels were synthesized from a solution consisting of 5% (w/v) NorHA, 1 mM lithium phenyl-2,4,6-trimethyl benzoylphosphinate (LAP) photoinitiator to induce thiyl radicals, and dithiothreitol (DTT) for crosslinking ([thiol]:[norbornene] = 0.6) in PBS. For each hydrogel, 50 μL of the NorHA solution was pipetted onto a thiol-functionalized glass coverslip (22 × 22 mm), sandwiched with an 18 × 18 mm coverslip, and crosslinked by irradiation for 2 min at 365 nm (10 mW cm^{-2}, Omnicure) to covalently stabilize the gel network. NorHA hydrogels to be used in spatial patterning experiments were incubated in a 1% (w/v) bovine serum albumin (BSA) solution in PBS for 30 min to limit nonspecific binding prior to subsequent experiments; NorHA hydrogels to be uniformly patterned were incubated solely in PBS prior to use in experiments.

2.5. Preparation of norbornene-functionalized polyethylene glycol (PEG-NB) electrospun fibers

The electrospinning protocol was adapted from Sharma and coworkers[24] and all fibers were collected on thiolated coverslips – identical to those used for preparing the 2D NorHA hydrogels. Solutions consisting of 8-arm PEG-NB (10% w/v, ~20 kDa, JenKem Technology, USA), polyethylene oxide (5% w/v, ~400 kDa, carrier polymer), DTT ([thiol] : [norbornene] = 0.6), and 2-hydroxy-4′-(2-hydroxyethoxy)-2-methylpropiophenone (I2959, 0.05% w/v) were mixed for at least 24 h in PBS. Electrospinning was conducted on a custom setup with the following parameters: 16-gauge needle; ~15 cm between the needle and collection surface; 0.8 mL h^{-1} flow rate; 10–14 kV positive voltage applied to the needle; and 6 kV negative voltage applied to the collection surface. Fibers were collected for at least 10 min and crosslinked for 15 min (365 nm, 10 mW cm^{-2}, Omnicure) under nitrogen. Fibers were then incubated in a 1% (w/v) BSA/PBS solution if they were to be spatially patterned or in PBS alone if they were to be uniformly patterned prior to subsequent experimentation.

2.6. Photoligation of peptides to hydrogels and fibers

NorHA hydrogels and PEG-NB fibers were fabricated with a 0.6 thiol : norbornene ratio to avail norbornene groups for photopatterned attachment of thiolated peptides after crosslinking. For fluorescent-based experiments (Fig. 2 and 3), solutions of thiolated peptides (20 μM, T-peptide or thiolated fluorophore), BSA (1% w/v), and LAP (1 mM) in PBS were added dropwise to the surface of the hydrogels/fibers, covered with photomasks (CAD/Art Services), and irradiated (365 nm, 10 mW cm^{-2}) for 2 min. For cell-based experiments (Fig. 4 and 5), a 100 μM solution of the T-peptide with 1 mM LAP in PBS was added dropwise to the surface of the hydrogels/fibers and irradiated with light (365 nm, 10 mW cm^{-2}) for 2 min. Following radical-induced thiol–ene coupling of the peptides to the hydrogel/fiber surfaces, samples were washed 3× in PBS for at least 30 min per wash to remove unreacted peptide and stored at room temperature until further use. Hydrogels/fibers with covalently tethered fluorophores were imaged directly after the wash steps, while other samples were used in coiled coil experiments as described below.

2.7. Formation of coiled coil complexes and subsequent peptide release

To induce coiled coil peptide complex formation on NorHA hydrogels and PEG-NB fibers, the scaffolds with tethered T-peptide were swollen with a 20 μM solution of the complementary A-peptide (2 mL per well) for 3 min prior to washing 3× with PBS for at least 30 min per wash to remove unbound peptide. To release the A-peptide, D-peptide was introduced into the system (3 mL per well, 20 μM for fluorescence experiments) at multiple time points. During the disruption process, the higher affinity D-peptide binds A-peptides, disrupting the A-peptide : T-peptide coiled coil and removing the A-peptides from the surface. Solution (1 mL) was removed at predetermined timepoints, and remaining 2 mL were aspirated off and replaced with fresh D-peptide solution. Aliquots collected at each time point were stored at 4 °C until analysis.

To introduce an Arg-Gly-Asp (RGD) cell adhesion motif into hydrogels and fibers for cell culture, 100 μM of the T-peptide was tethered to the substrates by the radical-induced thiol–ene click reaction as described above. Subsequently, following the same protocol as above, solutions of either 0 μM, 10 μM, or 100 μM of a complementary A-peptide containing an RGD sequence (GYGRGDSPG(KIAALKE)$_4$) were added to supramolecularly attach the adhesion motif to the surface. For disruption of this complex and removal of RGD from the system, 100 μM solutions of the D-peptide were used. For covalent RGD immobilization, a thiolated version of the RGD peptide (GCGYGRGDSPG, Genscript) was added to the surface at the designated RGD concentrations for photo-mediated thiol–ene attachment.

2.8. Determination of peptide release

Kinetics of peptide release from NorHA hydrogels were indirectly assessed using plate reader measurements of fluorophore intensity in the supernatant at time points during disruption. Briefly, the A-peptide was synthesized as described above with 5(6)-carboxyfluorescein (FAM) included on the N-terminus during peptide synthesis, and the fluorescence of the disruption solution at each time point was determined *via* a BioTek Synergy 4 fluorescence spectrophotometer (excitation: 495 nm; emission: 518 nm). Three hydrogels were assessed for each experimental group.

Peptide release was further assessed visually using fluorescence microscopy (Leica DMi8 Widefield) during disruption. At each time point, fluorescent images (20×, dry) were taken of each NorHA hydrogel and the average intensity of photopatterned stripes was determined *via* ImageJ pixel intensity analysis. Three stripes per hydrogel were measured across three hydrogels for each experimental group.

2.9. Cell culture

NIH 3T3 fibroblasts (kindly provided by Dr Steven Caliari at the University of Virginia) were used for all cell experiments (passages 4–8). Cells were cultured in Dulbecco's modified Eagle's medium (DMEM) fortified with 10% (v/v) calf bovine serum (ATCC) and 1× antibiotic-antimycotic (Gibco). Prior to seeding cells on 2D NorHA hydrogels or PEG-NB fibers, hydrogels and fibers were sterilized with germicidal light for 2 h and swelled with culture medium for at least 30 min. Cells suspended in culture medium were seeded at a density of 5×10^4 cells per hydrogel or fiber sample and allowed 24 h to adhere to the surface. Cells were then fixed for subsequent analysis, as described below.

For release experiments, hydrogel/fibrous scaffolds were similarly seeded at a density of 5×10^4 cells per scaffold, and cells were allowed to adhere for 24 h. Following the 24 h window, the medium was removed and replaced with culture medium containing D-peptide (2 mL, supplemented with 100 μM of the D-peptide) to induce release of the A-peptide.

The D-peptide-containing medium was exchanged a total of two times, with exchanges at 1 h intervals, to facilitate displacement of coiled-RGD peptide. An incubation time of 1 h was allowed after the second treatment for a cumulative 3 h window. Following this release cycle, cells were fixed and treated for subsequent analysis.

2.10. Cell staining

For analysis of cell experiments, fibroblasts were fixed in a 10% (v/v) solution of neutral buffered formalin for 15 min before permeabilization with a 0.1% (v/v) Triton X-100/PBS solution for 10 min. Samples were then blocked by incubation in a 3% (w/v) BSA solution for at least 1 h to prevent nonspecific binding. F-actin was visualized by staining with Alexa Fluor-488-phalloidin (Thermofisher, 1 : 600 dilution) for at least 1 h and nuclei were visualized by staining with DAPI (ThermoFisher, $1:1 \times 10^4$ dilution) for 1 min. Samples were washed once with PBS, once with 0.1% (v/v) TWEEN-20 in PBS, and again in PBS after the staining steps to remove unbound fluorophore. All samples were protected from light and stored at 4 °C until imaging.

2.11. Imaging and image analysis

All imaging was conducted on a Leica DMi8 Widefield microscope. Coverslips with NorHA hydrogels or PEG-NB fibers were placed on microscope slides, sandwiched with a 25 × 25 mm coverslip, and inverted for imaging. Imaging settings (exposure time and light intensity) were held constant for all imaging where fluorescence intensities were compared across multiple samples. For imaging of hydrogels containing fluorescent peptides, three distinct photopatterned stripes per scaffold from three scaffolds were imaged for analysis. Images acquired with the 20× dry objective were used for intensity comparisons. To evaluate pattern fidelity, we plotted the normalized intensity line profiles across 3 stripes on each sample; all intensity profiles were normalized to the lowest intensity value corresponding to each representative image.

For cellular experiments, at least three distinct areas per scaffold for three hydrogel and three fibrous scaffolds were imaged for cell spread area analyses. A 40× dry objective was used for cell area measurements, while a 100× oil immersion objective was used to visualize F-actin formation.

2.12. Statistical analyses

For quantitative comparisons between two experimental groups, independent *t*-tests were used; for comparisons with more than two experimental groups, a one-way ANOVA was leveraged in conjunction with a Tukey HSD *post-hoc* test with an α value of 0.95 indicating statistical significance.

3. Results and discussion

Hydrogels are advantageous for use in synthetic ECM-mimetic materials due to their high water content – similar to natural tissue – and tailorability to specific applications.[4,14] Moreover, many tissue-specific ECMs have fibrous components, and fibers are thus attractive *in vitro* models of physiological milieus.[4,14,49,50] Towards introducing spatiotemporally controlled signals within these model environments, we investigated the ability of supramolecular coiled coil complexes to facilitate dynamic presentation of molecular adhesion motifs on or within both 2D NorHA hydrogels and fibrous PEG-NB hydrogels.

Hyaluronic acid is a hydrophilic, non-sulfated glycosaminoglycan that is ubiquitous in natural ECM, and thus intrinsically biocompatible.[16,17] PEG is a hydrophilic, biocompatible synthetic polymer used widely for biomedical applications, including for solubilization of therapeutics and as components of ECM-mimetic hydrogels.[14,29] Both HA and PEG are amenable to chemical modification either on the side chains or at the chain ends.[14] We installed norbornene moieties on both HA and PEG (NorHA and PEG-NB, respectively) to enable efficient, spatially controlled photo-mediated thiol–ene click reactions for addition of thiolated cross-linkers and biomolecules.[18,24,51,52] The resulting NorHA hydrogels and PEG-NB fibers were crosslinked using dithiothreitol (DTT) as a crosslinker, adjusting the stoichiometry to leave residual norbornene groups available for post-crosslinking addition of thiolated peptides.[1,18,24]

Coiled coil-forming peptides were designed as shown in Scheme 1 based on a previously described complementary glutamic acid/lysine (E/K)-rich peptide pairs that form heterodimeric coiled coils[45,47,53] and undergo toehold-mediated strand displacement.[45] We sought to modify the sequences with cysteine residues to facilitate thiol–ene conjugation to NorHA and PEG-NB and demonstrate transfer of fluorophore or adhesive motif-tagged complementary peptides. For immobilization to the hydrogel surfaces, a tethered peptide (T-peptide) was designed with a cysteine for conjugation,[54] a glycine spacer, and three repeating heptads of EIAALEK as the glutamic acid (E)-rich coiled coil-forming motif (I = isoleucine, A = alanine, L = leucine).[45,47] The complementary association peptide (A-peptide) was designed with four repeating, lysine (K)-rich complementary KIAALKE heptads.[45,47] The extra heptad repeat provides a toehold motif for triggered removal of the A peptide in the presence of the higher affinity disruptor peptide (D-peptide) having four complementary repeating E-rich EIAALEK heptads.[45] We hypothesized that this difference in affinities would facilitate removal of A-peptides from the hydrogels by disrupting the A-peptide : T-peptide coiled coils upon introduction of the D-peptide in solution. We further extend this platform for dynamic incorporation of adhesive ligands (here, the fibronectin-derived RGD motif) for use in cell culture systems. To accomplish this, we modified the A-peptide with an RGD sequence ("coiled-RGD") at the N-terminus.

3.1. Thermodynamic characterization of coiled coil peptide interactions using isothermal titration calorimetry (ITC)

Prior to applying these peptides to NorHA hydrogels and PEG-NB fibers for reversible biomolecule attachment, their

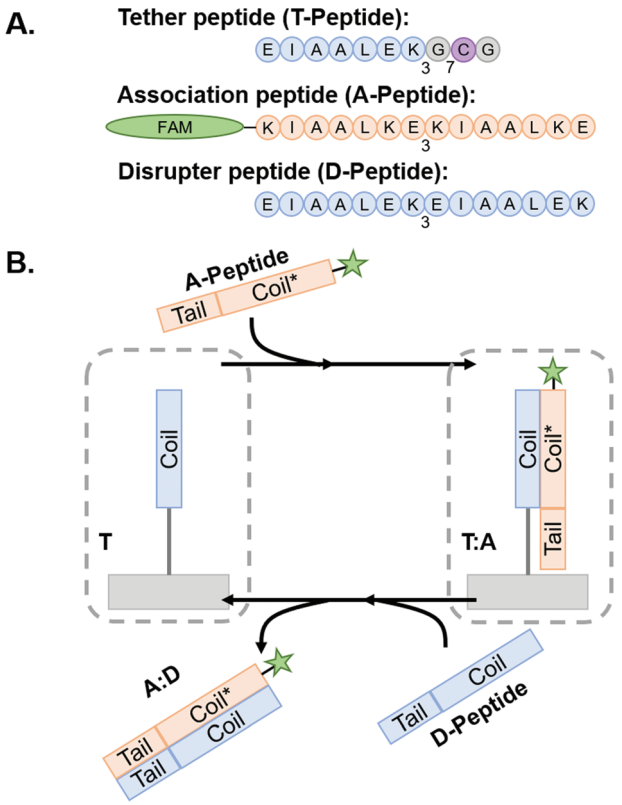

Scheme 1 Coiled coil peptides and process schematic of peptide association and subsequent removal *via* toehold-mediated strand displacement. (A) Representative peptides used in this study. Blue regions indicate E-rich coiled coil-forming heptads, orange regions indicate complementary k-rich heptads, and yellow regions indicate the toehold motifs. (B) Tethered peptides are covalently conjugated to NorHA/PEG-NB surfaces prior to incubation with A-peptide to form T : A coiled-coil complex. The system is then incubated with D-peptide to interrupt the complex and form the A : D coiled-coil – thus removing the FAM-tagged A-peptide from the hydrogel and leaving behind a vacant T-peptide. Figure inspired by Gröger *et al.*[45]

interactions when forming complexes were characterized using ITC. ITC is capable of assessing thermodynamic properties of associations in solution.[48,55] The coiled coil forming peptide pairs shown in Scheme 1 were analyzed in either NIH 3T3 fibroblast medium, PBS, or both, and representative baseline-subtracted thermograms and integrated data are shown in Fig. 1 for the complexes used in the cell culture studies – namely T-peptide : coiled-RGD peptide and coiled-RGD peptide : D-peptide, as well as a control experiment showing no interactions between non-complementary T-peptide and D-peptide pairs. Other replicates in medium, as well as PBS trials, are included in the ESI (Fig. S6–8† for medium and Fig. S9–13† for PBS).

Analysis of the ITC data in culture medium indicates that the T-peptide : coiled-RGD peptide forms two distinct, independent sites of interaction with strong affinities ($K_{D,1}$ ~10^{-7}–10^{-9} M, $K_{D,2}$ ~10^{-6}–10^{-7} M, represented in Fig. 1). This result is consistent with two-stage binding processes reported for coiled coils formed from peptides with mismatched lengths.[45,56] Conversely, ITC of the same two peptides without the RGD moiety (*i.e.*, T-peptide : A-peptide association) showed only one binding site (K_D ~10^{-6}, Fig. S9†). Therefore, the multiple binding sites are likely encouraged due to the presence of RGD causing a greater mismatch in peptide lengths. As noted by the K_D values, both sites of the T-peptide : coiled-RGD peptide complex exhibit strong binding affinities, which is advantageous for stable presentation of biomolecules.

Interestingly, the coiled-RGD peptide : D-peptide trace also seems to exhibit two-stage binding; however, the presence of both exothermic and endothermic heats of interaction prevents a model from fitting the data. This two-stage binding is intriguing as the coiled-RGD peptide and D-peptide both contain 4 coiled coil-forming heptad repeats. Therefore, the additional RGD residues yield mismatched lengths which may explain the multi-stage model. Moreover, these endothermic peaks may be indicative of higher order structures forming in solution, as has been reported for peptides that undergo self-complementary assembly.[57] Nevertheless, the larger magnitude of the heats of interaction from the coiled-RGD peptide : D-peptide interaction (~−80 kJ mol^{-1}, Fig. 1) compared to those of the T-peptide : coiled-RGD peptide (~−30 kJ mol^{-1}, Fig. 1) indicate that the coiled-RGD peptide : D-peptide complex is thermodynamically favored over the T-peptide : coiled-RGD peptide complex. Therefore, we conclude that the coiled-RGD peptide will preferentially interact with the D-peptide in the presence of the T-peptide – facilitating reversibility in our system.

The T-peptide : D-peptide analysis indicates no discernible interactions between the two peptides in solution, with heats of interaction of essentially 0 kJ mol^{-1} after correcting for the heats of dilution of T peptide into media and media into D-peptide. These results indicate that, as expected, the D-peptide does not interact with the T-peptide, and the D-peptide should displace the coiled-RGD peptide from the T-peptide : coiled-RGD peptide coiled coil due to the differences in their strengths of interaction – comparable to the results presented by Gröger *et al.*[45] using similar peptides to form coiled coils in solution.

These ITC experiments were also conducted in the presence of PBS to investigate how the absence of serum affects peptide complex affinities. The resultant ITC thermograms and integrated analyses (Fig. S9–13†) indicate only marginally different heats of interaction when PBS is used rather than cell culture medium.

3.2. Spatial patterning of FAM-tagged peptides onto NorHA hydrogels and PEG-NB hydrogel fibers

First, we tested the hypothesis that supramolecular coiled coil-mediated immobilization would yield similar patterns as covalent immobilization of fluorophores onto hydrogels. In these experiments, 100 μm-wide stripes were generated using a photomask and standard lithographic techniques.[1,10,18] Covalently bound fluorophores were introduced by patterning a thiolated FAM onto NorHA/PEG-NB surfaces (see Fig. 2A). For supramolecular patterning, unlabeled, thiolated T-peptide

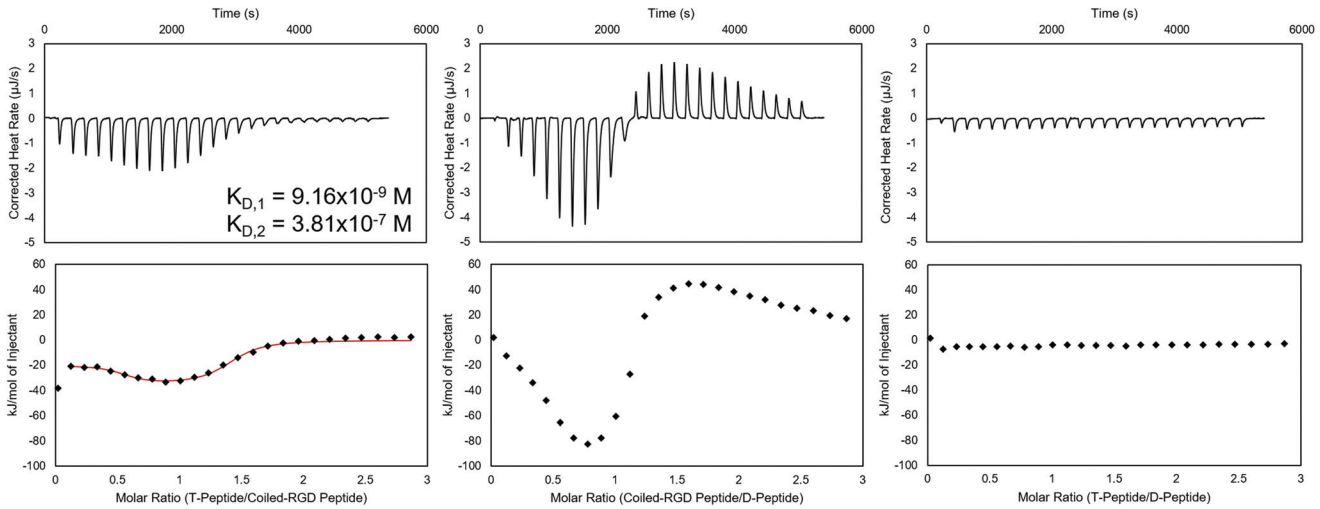

Fig. 1 Isothermal titration calorimetry of T-peptide : coiled-RGD peptide, coiled-RGD peptide : D-peptide, and T-peptide : D-peptide interactions in NIH 3T3 fibroblast medium. (Top) Baseline-subtracted ITC thermograms, integrated to yield the heats of interaction in kJ mol^{-1} (bottom plots). If possible, the integrated plots were fit to models (shown as a red line) that provide parameters for the interaction in solution. The T-peptide : coiled-RGD peptide complex exhibits high affinities, as evidenced by the K_D values on the order of 10^{-7}–10^{-9} M. The larger exothermic heats of interaction measured for the coiled-RGD peptide : D-peptide complex as compared to the T-peptide : coiled-RGD peptide complex demonstrate the greater strength of these interactions. No appreciable heats of interaction were observed for non-complementary T-peptide : D-peptide pairs.

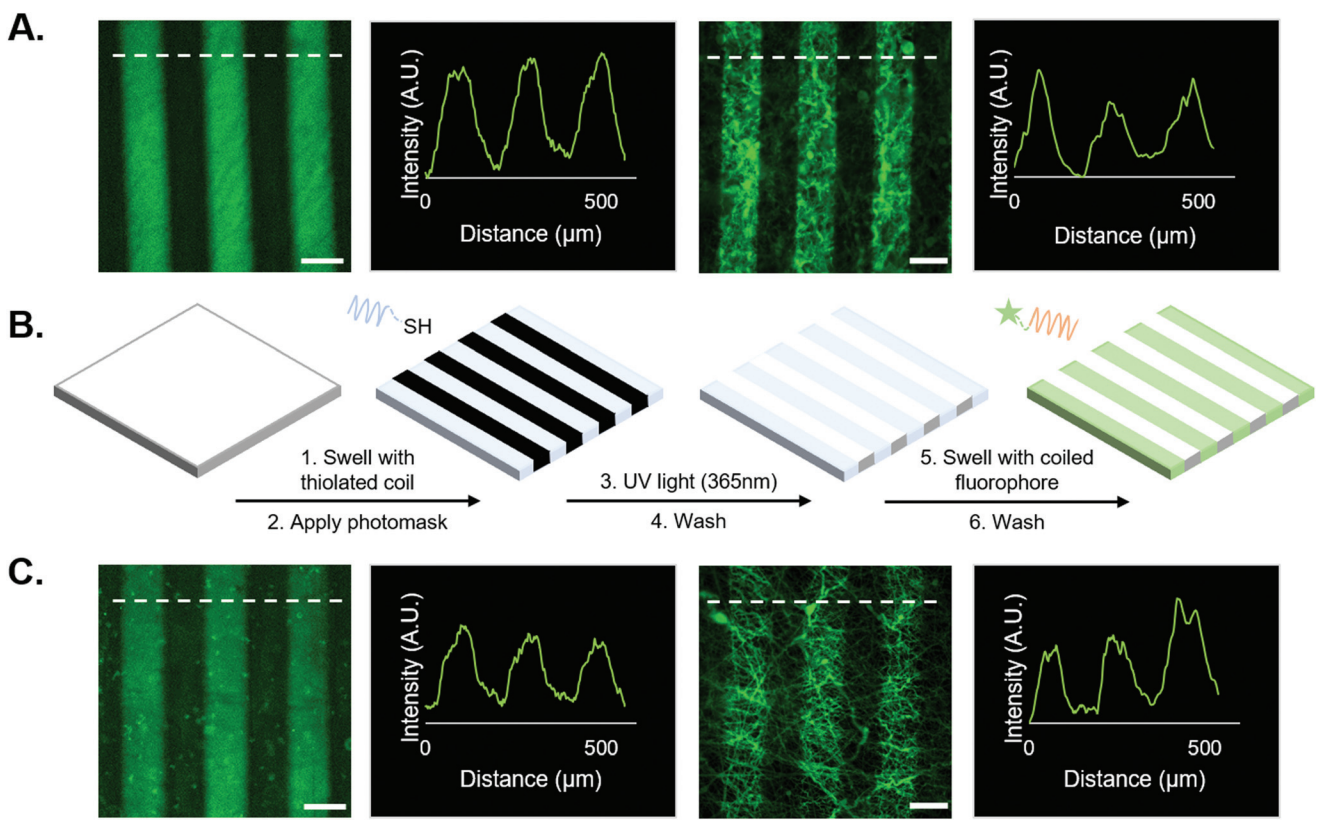

Fig. 2 Supramolecular *vs.* covalent immobilization of FAM on NorHA hydrogels and PEG-NB fibers. (A) Covalent system (from left to right): representative micrographs of covalently photopatterned FAM on a NorHA hydrogel; representative intensity line profile; representative micrograph of covalently bound FAM on PEG-NB fibers; representative intensity profile. (B) Schematic of the supramolecular patterning process for FAM utilizing our coiled-coil system: swelling of substrate – either 2D hydrogel or fibers –with thiolated T-peptide, application of photomask and irradiation with 365 nm light; substrate is then washed and swelled with the complementary FAM-tagged A-peptide; finally, substrate is then washed again to remove unbound peptide. (C) Coiled system (from left to right): representative micrograph of FAM bound by coiled-coil system on a NorHA hydrogel; representative intensity profile; representative micrograph of FAM bound by coiled-coil system on PEG-NB fibers; representative intensity profile. Scale bars = 100 μm. Dashed white lines indicate sample location of intensity profiles plotted for each micrograph.

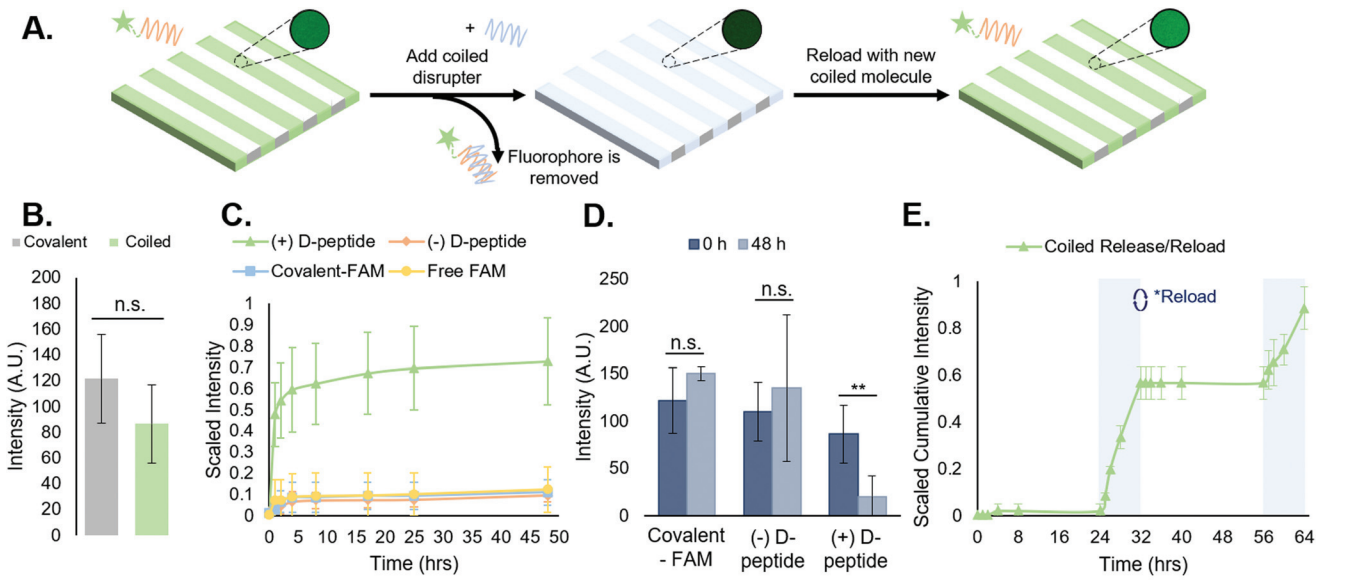

Fig. 3 Reversible, repeatable addition of biomolecules to peptide-functionalized hydrogels. (A) Schematic of FAM-tagged A-peptide release from substrates *via* toehold-mediated strand displacement upon addition of the complementary D-peptide, with inset images showing intensity- and exposure-controlled resultant changes in stripe fluorescence, with the ability to reload the vacant T-peptide sites in order to repeat the process. (B) Quantitative comparison of the average intensities of FAM by covalent and coiled-coil conjugations indicates no significant difference in stripe intensity between both platforms. (C) Cumulative release curves of the coiled coil disruption compared to the various controls. This indicates a coiled coil complex forming that is stable, with reversibility being disrupter-dependent. (D) Average stripe intensity at 0 h and 48 h time points, based on fluorescent micrographs, indicating a statistically significant difference (**$p < 0.01$) stripe intensity at 48 h for only the '(+) D-peptide' test group. (E) Repeated loading and release of FAM-tagged peptides from hydrogels shown by holding the hydrogels in PBS for 24 hours prior to inducing a D-peptide-dependent release for 8 h. Gels were then reloaded with A-peptide and the process was repeated. Profile shown is cumulative release from both disruption cycles. This further reinforces the notion that the system is stable over time in buffer and disruption can occur more than once *via* a release and reload protocol. Error bars represent standard deviation.

was first photopatterned onto NorHA and PEG-NB substrates, followed by incubation with a solution of the FAM-tagged complementary A-peptide. NorHA and PEG-NB scaffolds were washed with PBS to remove any unbound fluorophore prior to imaging (refer to Fig. 2B for a schematic of the process, and Fig. 2C for representative images). The resulting micrographs (Fig. 2) demonstrate that the NorHA and PEG-NB systems can be modified with fluorophore to generate stripe patterns either by covalent or supramolecular methods. The covalent systems typically yielded more uniform intensity profiles with higher peaks when compared to their coiled coil counterparts (Fig. 2A and C). Qualitatively, this can be visualized by the non-patterned regions of the coiled coil systems exhibiting more fluorescent signal than the covalent non-patterned regions. It is possible that steric hindrance near the surface limited uniform conjugation of FAM in the coiled coil system and/or that non-specific interactions between the hydrogel and peptides were greater when using coiled structures compared to the shorter peptides used in covalent conjugation.

Prior to the release studies, we compared the stripe intensities of the covalent and coiled coil systems to determine the system's net intensity under identical light conditions – analogous to a 'loading capacity' of prospective biomolecules. Analysis of stripe intensities from fluorescent micrographs indicated that although the average intensity of the coiled coil system was marginally lower than the covalent system, an independent *t*-test suggests there is no statistical significance (Fig. 3B). Therefore, our platform for supramolecular addition of biomolecules generates patterned stripes similarly to its covalent ligation analog at the experimental (20 μM) concentrations, allowing equivalent conjugation of fluorophore based on our semi-quantitative analysis.

3.3. Supramolecular immobilization of FAM *via* coiled coil peptide complexes is reversible and repeatable

Following experiments demonstrating spatially controlled supramolecular addition of FAM-tagged peptides to hydrogels using the coiled coil system, we sought to evaluate its efficacy as a reversible, repeatable process towards temporally controlled presentation of biomolecules on and in cell culture substrates.

We measured FAM concentration in solution as a function of time to determine the stability of the supramolecular coiled coil structure in buffer over time and monitor the toehold-mediated disruption of the complexes by adding the disrupter peptide (Fig. 3A). All release studies were performed on NorHA hydrogels due to the ability to precisely and reproducibly form substrates with consistent surface area across samples, enabling a closer comparison across all groups. First, we examined the release of the FAM-tagged A-peptide in the presence of the D-peptide (hereafter "(+) D-peptide"). Plate reader fluorescence measurements of supernatant samples indicated a

large cumulative release in the (+) D-peptide test group, suggesting that release is dependent on the addition of the D-peptide to disrupt the T : A coiled coil. To support this conclusion, we compared the (+) D-peptide test group to various controls. These controls consisted of a coiled coil system that was not subjected to D-peptide treatment (hereafter "(−) D-peptide"), a covalently bound FAM (hereafter "covalent-FAM"), and the FAM molecule in solution ("free-FAM"). The (−) D-peptide group was designed to evaluate supramolecular complex stability in buffer for extended periods of time (~48 h), and the free-FAM control was designed to determine the extent of non-specific interactions between the fluorophore in solution with the T-peptide-modified substrates. Using standard plate reader fluorescence measurements of supernatant samples, we measured FAM release profiles. The results indicated large cumulative release from the coiled coil group in comparison to controls that exhibited minimal, if any, release of fluorescent molecules (Fig. 3C). Furthermore, the supramolecular coiled coils persist over days in the absence of the D-peptide, indicating that this system can stably, but reversibly, incorporate biomolecules onto norbornene-modified hydrogels. The free-FAM control contained no stripes to quantify in subsequent analysis, suggesting no discernable interactions between the free molecule and the T-peptide surface.

To further quantify the release of the FAM-tagged A-peptide *via* addition of the disrupter, we looked at the average stripe intensities of the '(+) D-peptide' test group compared to the (−) D-peptide and 'covalent-FAM' controls at the first and last time points to compare the decrease in intensity upon FAM release. There were no significant differences between the stripe intensities at the first and last timepoints (0 h and 48 h) for the controls (Fig. 3D). However, the (+) D-peptide test group showed a statistically significant reduction in intensity after D-peptide treatment (**$p < 0.01$). Together, these data confirm the hypotheses that: (1) coiled coil peptides enable supramolecular immobilization on hydrogels; and (2) introduction of the D-peptide facilitates removal of supramolecularly immobilized molecules by toehold-mediated strand displacement.

We further investigated how different concentrations of D-peptide affected removal of the FAM-tagged A-peptide (Fig. S14†). Increasing concentrations of D-peptide generally enhanced and accelerated removal of the FAM-tagged A-peptide from the hydrogel surfaces; however, we began to observe diminishing increases in removal at higher concentrations of D-peptide. We postulate that at these higher concentrations, kinetics of peptide displacement might limit reversibility in the system over availability of D-peptide, with steric hindrances imposed by NorHA surfaces possibly limiting reversibility as well. Thus, increasing the concentration of D-peptide has the most significant effects on increasing A-peptide removal at lower concentrations of D-peptide, with only marginal improvement at higher concentrations of the competitive disrupter. Additionally, removal of A-peptide from T : A coiled coils in the presence of 3T3 fibroblast medium was investigated as a precedent for subsequent cell studies. Shown in Fig. S14,† removal in culture medium is similar to removal in PBS. Combining this observation with ITC measurements (Fig. S6–8†), we conclude that the specific and dynamic properties of the coiled-coil system extend to protein-rich environments, such as cell media.

Toehold-mediated removal of the A-peptide by addition of the complementary, higher affinity D-peptide leaves T-peptide sites vacant on the surface of NorHA hydrogels for binding other bioactive molecules. As a proof-of-concept, after release of the initially bound FAM-tagged A-peptide, we incubated the same scaffolds with a fresh solution of FAM-tagged A-peptide and rinsed the substrates with PBS to remove unbound peptide. After a 24 h incubation in PBS, D-peptide was reintroduced to cue a second removal of FAM-tagged peptide to demonstrate the repeatability of the process (Fig. 3E). The second release profile (t = 56–64 h) resembled the first (t = 24–32 h), albeit with a slightly smaller magnitude of cumulative release. These results suggest that this is a reversible and repeatable process, but we can also postulate that the D-peptide does not completely remove the A-peptide (Fig. 3D, where the '(+) D-peptide' group does not return to a 0-intensity value following disruption). This may be due to interactions with the NorHA surface that sterically interfere with removal, interactions with material in the gels that prevent reaching 100% removal, or equilibrium of toehold-mediated strand displacement.

3.4. Supramolecular, coiled coil-mediated immobilization of RGD confers bioactivity that supports 3T3 fibroblast adhesion to NorHA hydrogels and PEG-NB fibers with comparable morphologies to traditional covalent ligation

After using FAM-tagged A-peptides as a proof-of-concept to establish the viability of coiled coils for immobilization of biomolecules onto NorHA hydrogels and PEG-NB fibers, we next incorporated the cell-adhesive RGD-containing peptide sequence GYGRGDSPG into the A-peptide at the N-terminus to impart cell adhesive properties.[1] Here, photopatterned T-peptide hydrogels bound RGD-functionalized A-peptide ("coiled-RGD"). A thiolated version of the RGD peptide (GCGYGRGDSPG) was also covalently bound to NorHA and PEG-NB substrates for comparisons against our coiled coil system. To test cell behavior on scaffolds displaying the RGD motif, we cultured NIH 3T3 fibroblasts on NorHA hydrogels and PEG-NB fibers previously modified with different RGD concentrations (0, 10, 100 μM RGD *via* coiled coil or covalent conjugation). After incubation for 24 h, the samples were fixed and stained for fluorescent visualization of F-actin and cell nuclei, and cell area quantified. See Fig. 4A for cell area quantification and 3B/C for fluorescent micrographs of NorHA gels and PEG-NB fibers, respectively.

3.4.1. 3T3 Fibroblast behavior on covalent and coiled coil presentation of RGD on NorHA Hydrogels. As expected, images of 3T3 fibroblasts cultured on RGD-presenting substrates showed larger cell area, indicative of cell spreading. Increasing covalent RGD presentation from 0 μM to 10 μM and 100 μM increased cell spreading, with the 100 μM groups exhibiting statistically significant differences in cell area compared

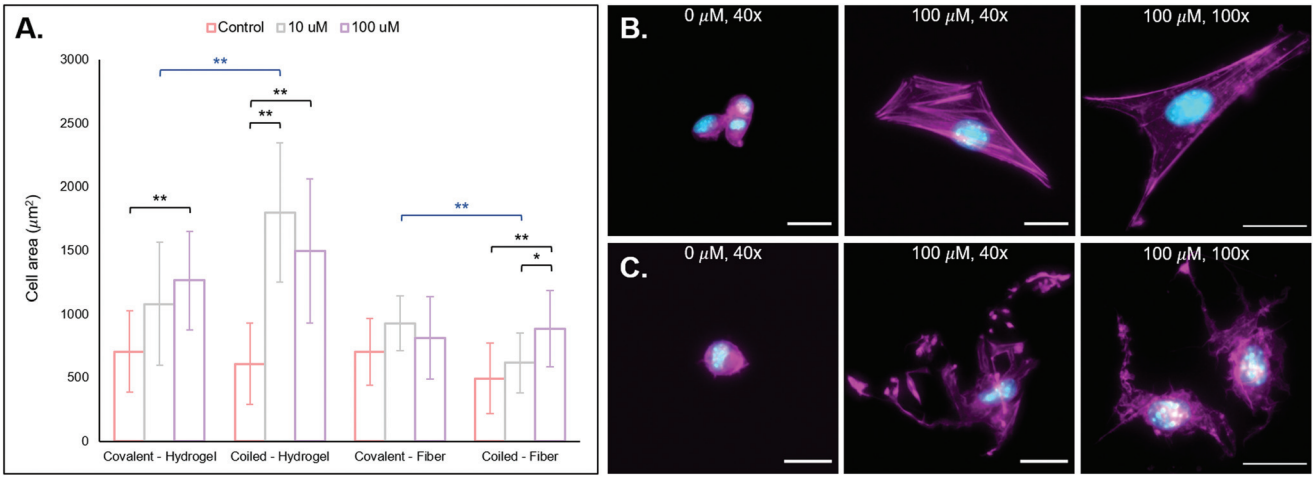

Fig. 4 3T3 fibroblast behavior on substrates with presentation of RGD through the coiled-coil platform. (a) Quantifications of cell area for each of the groups with comparisons to their covalently conjugated analogs. (b) NorHA 2D hydrogel (from left to right): 0 μm RGD, 100 μm RGD, and 100 μm RGD hydrogel zoomed in to better visualize cell structure. (c) PEG-NB hydrogel fibers (from left to right): 0 μm RGD, 100 μm RGD, and 100 μm RGD fibers zoomed in to better view cell structure. It is clear qualitatively from the images, and quantitatively from the cell area comparisons, that generally the addition of the coiled RGD peptide to the substrates improves bioactivity, and thus cell area increases. Furthermore, it is important to note that the F-actin stress fibers are more organized for cells on NorHA scaffolds than those on PEG-NB fibers. Scale bars = 25 μm, $^{**}p < 0.01$, $^{*}p < 0.05$. Error bars represent standard deviation.

to substrates exposed to 0 μM covalent RGD (Fig. 4A, $^{**}p < 0.01$). In our supramolecular system, the 10 μM coiled coil presentation of RGD significantly increases cell area ($^{**}p < 0.01$) compared to the 0 μM control, as does the 100 μM treatment ($^{**}p < 0.01$). Indeed, at low concentrations of ligand presentation, it is known that fibroblast cell area responds positively with increased ligand concentration.[58] Yet, we observe a marginally smaller average area with the 100 μM group compared to the 10 μM group (Fig. 4A). Similar results in the literature attribute this phenomenon to integrin inhibition due to free RGD in solution.[41,59] However, owing to the strong interactions between the T-peptide and the coiled-RGD in this system (K_D ~10^{-7}–10^{-9} in culture medium), it is likely that the observed differences in cell areas between the 10 μM and 100 μM groups are due to a combination of RGD density and gel mechanics. Oria *et al.*[60] demonstrate a bimodal relationship between the spacing of ECM ligands, which are controlled here by the concentration of the coiled-RGD, and substrate mechanics – with their interplay affecting focal adhesion formation. At the hydrogel mechanics used within this study, distance between the RGD ligands in the 10 μM groups may promote spreading and focal adhesion formation, and distances between ligands in the 100 μM groups may inhibit cell spreading and focal adhesion formation due to their proximity to one another.[60] Cell spreading and highly organized F-actin stress fibers within the RGD-presenting coiled coil system can be seen in representative images of the 0 μM and 100 μM groups (Fig. 4B) – likely a function of the high surface concentration of RGD allowing filopodia attachment during spreading and migration.[61]

We also observe generally larger cell areas for the 10 μM and 100 μM RGD groups with our coiled coil system compared to the covalent groups, with a statistically significant difference between the 10 μM supramolecular and covalent groups ($^{**}p < 0.01$). We hypothesize that this is likely due to the non-covalent, supramolecular characteristics of our coiled coil system that potentially allows cellular remodeling of RGD ligands within its environment. A covalent conjugation permanently immobilizes a pendant ligand on a substrate, allowing cells to exert traction forces.[62,63] These traction forces are ubiquitous and implicated in dynamic tissue processes (*e.g.* contraction),[62–64] and they may induce remodeling of the supramolecular coiled coil system. Since the conjugated T-peptide provides open and dynamic sites for coiled coil complexes to form, we postulate that cells may be able to reorganize the physical locations of the A-peptide motifs on the NorHA hydrogel surface through traction forces – thus providing a dynamic surface that leads to increased cell area. Dynamic interactions with 2D surfaces and 3D hydrogel matrices are known to play important roles in cell fate processes,[65–67] and supramolecular functionalization of materials may allow for ongoing, cell-mediated changes in surface properties.

3.4.2. 3T3 behavior on covalent and coiled coil presentation of RGD on PEG-NB Fibers. Similar to NorHA hydrogel groups, we also observed increased cell spreading on PEG-NB fibers that present RGD covalently and supramolecularly (after application of 10 and 100 μM RGD) compared to the 0 μM RGD controls (Fig. 4). Interestingly, cell spreading on PEG-NB fibers to which RGD was covalently conjugated was not significantly greater than spreading on the control fibers, although there appeared to be a slight increase in cell area for both groups compared to the 0 μM control (Fig. 4A). Like the covalently bound RGD on PEG-NB fibers, the supramolecular

immobilization of RGD on fibers exhibited modest differences in cell areas between the 0 μM and 10 μM groups, but demonstrated statistically larger cell areas in the 100 μM group compared to the unfunctionalized control (**p < 0.01). Furthermore, coiled coil complexes on fibers induced cells to spread significantly more in the 100 μM group compared to the 10 μM group (*p < 0.05). Cell area also decreased in moving from the experimental group of 10 μM RGD (in solution) covalently bound to fibers to the group of 10 μM RGD reversibly bound to fibers *via* coiled coil conjugation (**p < 0.01). Representative fluorescent micrographs of cell spreading and F-actin formation on PEG-NB fibers are shown in Fig. 4C.

In considering both materials systems, we observe that the supramolecular addition of the coiled RGD ligand promotes 3T3 fibroblast adhesion and spreading on both NorHA hydrogels and PEG-NB fibers, and it presents a generalizable method for temporally-controlled functionalization of hydrogel substrates for cell adhesion in further studies.

3.5. The addition of the D-peptide induces removal of the coiled adhesive motif which actuates changes in cell morphology

After demonstrating that cells can adhere and spread on substrates supramolecularly functionalized with coiled-RGD, we sought to investigate the effects of its removal *via* the addition of the competing D-peptide on cell adherence and morphology. Both the NorHA hydrogel and PEG-NB hydrogel fiber systems exhibited changes in cell adherence that could be observed qualitatively upon the addition of the D-peptide (Fig. 5A and B). Quantitatively, we saw significant changes in cell areas in both systems, with cell areas on the NorHA hydrogels decreasing by roughly 50% and cell areas on the PEG-NB fibers decreasing to the same sizes as seen on unmodified PEG-NB fibers (Fig. 5C).

3.5.1. Removal of coiled-RGD peptide from NorHA hydrogels. We saw statistically significant decreases in fibroblast area on the NorHA hydrogel substrates modified with 10 μM RGD after incubation with D-peptide (**p < 0.01, Fig. 5C). There was a significant reduction of cell area from an average of 1800 ± 550 μm^2 on the 10 μM scaffolds prior to release to an average of 910 ± 330 μm^2 afterwards. Average cell area after RGD release was still significantly larger than average area observed in the control groups of 610 ± 320 μm^2 (0 μM RGD, *p < 0.05, Fig. 5C). Based on observations discussed previously, we attribute this to steric hindrance and molecular interactions in the hydrogel that may inhibit D-peptide from fully displacing and removing the coiled-RGD motifs from the T-peptide, and also to thermodynamic equilibrium of toehold-mediated strand displacement, by which some A-peptide would be expected to remain associated with T-peptide even in the presence of D-peptide. Moreover, it is possible that due to the 24 h culture period prior to addition of the D-peptide, fibroblasts developed interactions with the NorHA gels that were difficult to disrupt – possibly through extended cellular interactions across the gel surface and into the gel itself – as well as nascent matrix deposition from the fibroblasts that might become integrated with the hydrogel surface.[68] Interestingly, there were also noticeably more cell clusters fol-

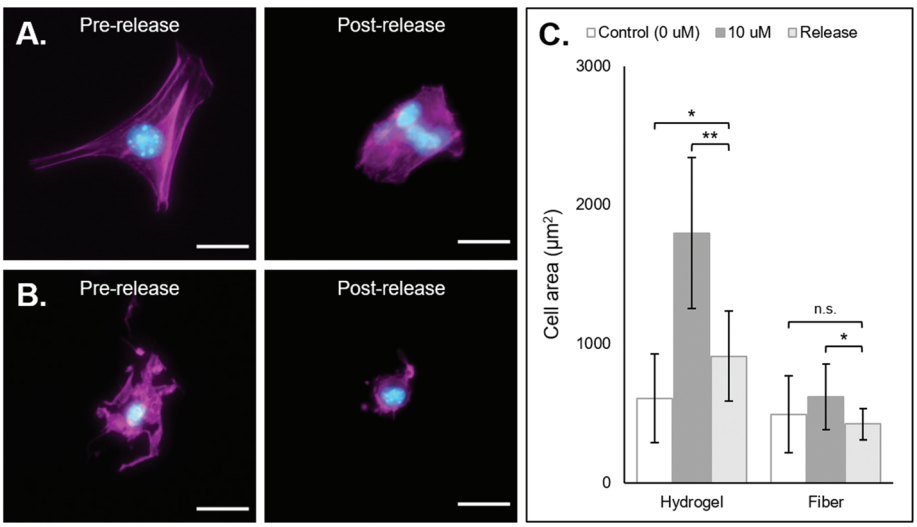

Fig. 5 3T3 morphology changes following removal of coiled-RGD peptide *via* the addition of the competing D-peptide. (A) NorHA hydrogel (from left to right): representative fluorescent micrograph of a fibroblast seeded on a NorHA hydrogel functionalized with 10 μm of the coiled-RGD motif; representative fluorescent micrograph of fibroblasts on a NorHA hydrogel originally functionalized with 10 μm of the coiled-RGD motif and treated with 100 μm of the D-peptide. Cells exhibited fewer extensions and appeared to aggregate. (B) PEG-NB fibers (left to right): representative fluorescent micrograph of a fibroblast seeded on PEG-NB fibers functionalized with 10 μm of the coiled-RGD motif; representative fluorescent micrograph of a fibroblast on PEG-NB fibers originally functionalized with 10 μm of the coiled-RGD motif and treated with 100 μm of the D-peptide. Cells exhibited fewer extensions and covered less surface area. (C) Quantification of cell area across groups in release experimentation. Statistics solely compared cell area after treatment with D-peptide to the control and 10 μm coiled-RGD groups prior to treatment with D-peptide. Scale bars = 25 μm, n.s. = no significance, *p < 0.05, **p < 0.01, error bars represent standard deviation.

lowing removal of the coiled-RGD ligands – suggesting that cells aggregate and adhere to other cells when concentrations of available RGD decrease. This observation correlates to cell clusters seen here with 0 μM RGD (refer to representative micrograph in Fig. 4B) and to work by Dumbleton and co-workers who demonstrated multiple cell types clustering on unfunctionalized hydrogels.[69] Furthermore, the behavior is analogous to work by Freeman *et al.*, who demonstrated the ability to remove adhesive laminin-derived IKVAV-peptide ligands from hydrogel surfaces and showed that neural stem cells tended to cluster in neurospheres once these ligands were removed from the culture surface.[43]

3.5.2. Removal of coiled-RGD peptide from PEG-NB fibers. We also observed a statistically significant decrease in fibroblast area on PEG-NB fibers after incubation with D-peptide compared to cells on the 10 μM scaffolds prior to incubation with D-peptide ($*p < 0.05$, Fig. 5C). Interestingly, there was no statistical significance in cell area between the scaffolds after removal of the coiled RGD from the 10 μM scaffolds and the 0 μM control scaffolds, indicating that the introduction of the D-peptide to the systems removed enough of the coiled-RGD peptide to return cell morphology to a state similar to the unfunctionalized control. Just as we observed in the NorHA hydrogel system, treatment with the D-peptide reversed adhesion of cells to the culture substrate through disrupting coiled coil interactions between the T- and RGD-containing A-peptides. We also note that differences in trends between the NorHA hydrogel and electrospun PEG-NB fibers, for example, the relative extent to which cell spreading was reversed. This might be attributed to factors including differences in the polymer backbone chemistries, differences in molecular concentration after processing a hydrogel by electrospinning, cellular responses to different topographies, or changes in viscoelastic properties or ligand densities between systems.

Nonetheless, overall changes in cell adhesion and morphology were temporally controlled *via* the addition of the D-peptide to displace the coiled-RGD in both NorHA and PEG-NB systems. This demonstrates the potential for user-controlled perturbation of cellular microenvironments. Taken together with previous results, this coiled coil system offers both spatial and temporal control over patterning of ligands that can affect cell behaviors.

4. Conclusions and outlook

Coiled coil peptides offer a versatile system for engineering spatial and temporal signals into hydrogel environments. Biofunctionality of a peptide can readily be altered through standard peptide synthesis techniques, and thiol groups in cysteine residues allow their incorporation *via* light-controlled reactions amenable to spatial patterning, as well as by other bioconjugation reactions, such as Michael additions. The supramolecular coiled coil interaction also presents a reversible platform that allows for the repeated introduction and removal of bioactivity within *in vitro* hydrogel and hydrogel fiber culture systems. Proof-of-concept experiments showing reversible immobilization of FAM demonstrated comparable efficacy in functionalizing photoreactive biomaterials with high spatial control using coiled coil complexes compared to covalent photoligations. We confirmed the stability of the supramolecular coiled coil association over time, with release being dependent on toehold-mediated strand displacement by the D-peptide – a process that can be repeated after subsequent reloading with A-peptide. We then developed an extension of the A-peptide that included a cell-adhesive RGD motif on the N-terminus. Using this coiled-RGD for cell studies illustrated the ability to culture fibroblasts on materials functionalized with RGD *via* this coiled coil system. The concentration of the coiled-RGD peptide bound to the T-peptide affected the cell spread area on both NorHA hydrogels and PEG-NB fibers. Finally, removal of the coiled-RGD *via* introduction of the D-peptide caused a statistically significant decrease in cell spread area – on both hydrogels and fibers – indicating that the reversal of RGD presentation has a direct impact on fibroblast morphology. On the basis of these observations, future work should allow for the investigation of how dynamism in cell culture environments affects downstream cell behaviors. User-defined perturbations to these culture environments will allow for incremental advancements based on discrete changes to the microenvironment. Future work will also consider differences in cell behaviors on hydrogels and hydrogel-based fibers, as well as differences between hydrogel backbone materials in this system. We believe this platform might be applied to many other areas of research that desire user-controlled addition and subsequent temporal release of bioactive compounds that can be reloaded for multiple release cycles.

Conflicts of interest

There are no conflicts to declare.

Acknowledgements

The authors would like to Dr Steven R. Caliari at the University of Virginia for providing the NIH 3T3 fibroblasts as well as usage of the BioTek Synergy 4 spectrophotometer. Furthermore, the authors would like to thank Dr Nicholas E. Sherman for usage of circular dichroism spectroscopy and for conducting electrospray ionization mass spectrometry in the Biomolecular Analysis Facility which is supported by the University of Virginia School of Medicine.

This work was supported by the University of Virginia and the National Institutes of Health through UVA Biotechnology Training Program NIGMS 5T32 GM008715 and GM136615. The content is solely the responsibility of the authors and does not necessarily represent the official views of the National Institutes of Health.

References

1 R. J. Wade, E. J. Bassin, W. M. Gramlich and J. A. Burdick, *Adv. Mater.*, 2015, **27**, 1356–1362.
2 B. M. Baker, B. Trappmann, W. Y. Wang, M. S. Sakar, I. L. Kim, V. B. Shenoy, J. A. Burdick and C. S. Chen, *Nat. Mater.*, 2015, **14**, 1262–1268.
3 C. D. Davidson, W. Y. Wang, I. Zaimi, D. K. P. Jayco and B. M. Baker, *Sci. Rep.*, 2019, **9**, 12.
4 B. M. Baker and C. S. Chen, *J. Cell Sci.*, 2012, **125**, 3015–3024.
5 R. J. Wade and J. A. Burdick, *Mater. Today*, 2012, **15**, 454–459.
6 A. Velasco-Hogan, J. Xu and M. A. Meyers, *Adv. Mater.*, 2018, **30**(52), 1800940.
7 B. Grigoryan, S. J. Paulsen, D. C. Corbett, D. W. Sazer, C. L. Fortin, A. J. Zaita, P. T. Greenfield, N. J. Calafat, J. P. Gounley, A. H. Ta, F. Johansson, A. Randles, J. E. Rosenkrantz, J. D. Louis-rosenberg, P. A. Galie, K. R. Stevens and J. S. Miller, *Science*, 2019, **364**, 458–464.
8 C. Frantz, K. M. Stewart and V. M. Weaver, *J. Cell Sci.*, 2010, **123**, 4195–4200.
9 M. P. Lutolf and J. A. Hubbell, *Nat. Biotechnol.*, 2005, **23**, 47–55.
10 R. J. Wade, E. J. Bassin, C. B. Rodell and J. A. Burdick, *Nat. Commun.*, 2015, **6**, 6639.
11 C. A. Deforest and K. S. Anseth, *Angew. Chem., Int. Ed.*, 2012, **51**, 1816–1819.
12 J. C. Grim, I. A. Marozas and K. S. Anseth, *J. Controlled Release*, 2015, **219**, 95–106.
13 M. M. Stevens and J. H. George, *Science*, 2005, **310**, 1135–1138.
14 S. R. Caliari and J. A. Burdick, *Nat. Methods*, 2016, **13**, 405–414.
15 M. W. Tibbitt and K. S. Anseth, *Biotechnol. Bioeng.*, 2009, **103**, 655–663.
16 C. B. Highley, G. D. Prestwich and J. A. Burdick, *Curr. Opin. Biotechnol.*, 2016, **40**, 35–40.
17 J. A. Burdick and G. D. Prestwich, *Adv. Healthcare Mater.*, 2011, **23**, H41–H56.
18 W. M. Gramlich, I. L. Kim and J. A. Burdick, *Biomaterials*, 2013, **34**, 9803–9811.
19 E. Hui, K. I. Gimeno, G. Guan and S. R. Caliari, *Biomacromolecules*, 2019, **20**, 4126–4134.
20 J. A. Burdick and W. L. Murphy, *Nat. Commun.*, 2012, **3**, 1269.
21 C. D. Davidson, D. K. P. Jayco, D. L. Matera, S. J. DePalma, H. L. Hiraki, W. Y. Wang and B. M. Baker, *Acta Biomater.*, 2020, **105**, 78–86.
22 S. A. Fisher, R. Y. Tam, A. Fokina, M. M. Mahmoodi, M. D. Distefano and M. S. Shoichet, *Biomaterials*, 2018, **178**, 751–766.
23 R. Y. Tam, L. J. Smith and M. S. Shoichet, *Acc. Chem. Res.*, 2017, **50**, 703–713.
24 S. Sharma, M. Floren, Y. Ding, K. R. Stenmark, W. Tan and S. J. Bryant, *Biomaterials*, 2017, **143**, 17–28.
25 J. J. Roberts and S. J. Bryant, *Biomaterials*, 2013, **34**, 9969–9979.
26 C. E. Hoyle and C. N. Bowman, *Angew. Chem., Int. Ed.*, 2010, **49**, 1540–1573.
27 O. I. Kalaoglu-Altan, B. Verbraeken, K. Lava, T. N. Gevrek, R. Sanyal, T. Dargaville, K. De Clerck, R. Hoogenboom and A. Sanyal, *ACS Macro Lett.*, 2016, **5**, 676–681.
28 C. A. Deforest and D. A. Tirrell, *Nat. Mater.*, 2015, **14**, 523–531.
29 J. C. Grim, T. E. Brown, B. A. Aguado, D. A. Chapnick, A. L. Viert, X. Liu and K. S. Anseth, *ACS Cent. Sci.*, 2018, **4**, 909–916.
30 G. Weng, U. S. Bhalla and R. Iyengar, *Science*, 1999, **284**, 92–97.
31 C. Xie, W. Sun, H. Lu, A. Kretzschmann, J. Liu, M. Wagner, H. J. Butt, X. Deng and S. Wu, *Nat. Commun.*, 2018, **9**, 1–9.
32 F. M. Fumasi, N. Stephanopoulos and J. L. Holloway, *J. Appl. Polym. Sci.*, 2020, **137**, 1–16.
33 A. M. Kloxin, A. M. Kasko, C. N. Salinas and K. S. Anseth, *Science*, 2009, **324**, 59–63.
34 L. Liu, X. Tian, Y. Ma, Y. Duan, X. Zhao and G. Pan, *Angew. Chem., Int. Ed.*, 2018, **57**, 7878–7882.
35 J. L. Mann, A. C. Yu, G. Agmon and E. A. Appel, *Biomater. Sci.*, 2018, **6**, 10–37.
36 E. A. Appel, F. Biedermann, U. Rauwald, S. T. Jones, J. M. Zayed and O. A. Scherman, *J. Am. Chem. Soc.*, 2010, **132**, 14251–14260.
37 C. B. Highley, C. B. Rodell and J. A. Burdick, *Adv. Mater.*, 2015, **27**, 5075–5079.
38 E. A. Appel, X. J. Loh, S. T. Jones, F. Biedermann, C. A. Dreiss and O. A. Scherman, *J. Am. Chem. Soc.*, 2012, **134**(28), 11767–11773.
39 J. D. Tang, C. Mura and K. J. Lampe, *J. Am. Chem. Soc.*, 2019, **141**, 4886–4899.
40 C. B. Highley, C. B. Rodell, I. L. Kim, R. J. Wade and J. A. Burdick, *J. Mater. Chem. B*, 2015, **2**, 8110–8115.
41 J. Boekhoven, C. M. Rubert Pérez, S. Sur, A. Worthy and S. I. Stupp, *Angew. Chem., Int. Ed.*, 2013, **52**, 12077–12080.
42 S. L. McNamara, Y. Brudno, A. B. Miller, H. O. Ham, M. Aizenberg, E. L. Chaikof and D. J. Mooney, *ACS Biomater. Sci. Eng.*, 2020, **6**(4), 2159–2166.
43 R. Freeman, N. Stephanopoulos, Z. Álvarez, J. A. Lewis, S. Sur, C. M. Serrano, J. Boekhoven, S. S. Lee and S. I. Stupp, *Nat. Commun.*, 2017, **8**, 15982.
44 R. Freeman, M. Han, Z. Alvarez, J. A. Lewis, J. R. Wester, N. Stephanopoulos, M. T. McClendon, C. Lynsky, J. M. Godbe, H. Sangji, E. Luijten and S. I. Stupp, *Science*, 2018, **813**, 808–813.
45 K. Gröger, G. Gavins and O. Seitz, *Angew. Chem., Int. Ed.*, 2017, **201705339**, 14217–14221.
46 A. N. Lupas and M. Gruber, *Adv. Protein Chem.*, 2005, **70**, 37–78.
47 J. R. Litowski and R. S. Hodges, *J. Biol. Chem.*, 2002, **277**, 37272–37279.

48 W. R. Archer and M. D. Schulz, *Soft Matter*, 2020, **16**, 8760–8774.
49 R. J. Wade and J. A. Burdick, *Nano Today*, 2014, **9**, 722–742.
50 C. D. Davidson, D. K. P. Jayco, W. Y. Wang, A. Shikanov and B. M. Baker, *J. Biomech. Eng.*, 2020, **142**, 1–9.
51 M. Iglesias-Echevarria, L. Durante, R. Johnson, M. Rafuse, Y. Ding, W. Bonani, D. Maniglio and W. Tan, *Biomater. Sci.*, 2019, **7**, 3640–3651.
52 A. M. Kloxin, C. J. Kloxin, C. N. Bowman and K. S. Anseth, *Adv. Mater.*, 2010, **22**, 3484–3494.
53 B. Apostolovic and H. A. Klok, *Biomacromolecules*, 2008, **9**, 3173–3180.
54 D. P. Nair, M. Podgórski, S. Chatani, T. Gong, W. Xi, C. R. Fenoli and C. N. Bowman, *Chem. Mater.*, 2014, **26**, 724–744.
55 M. Kabiri and L. D. Unsworth, *Biomacromolecules*, 2014, **15**, 3463–3473.
56 G. De Crescenzo, J. R. Litowski, R. S. Hodges and M. D. O'Connor-McCourt, *Biochemistry*, 2003, **42**, 1754–1763.
57 M. Kabiri, I. Bushnak, M. T. McDermot and L. D. Unsworth, *Biomacromolecules*, 2013, **14**, 3943–3950.
58 C. Gaudet, W. A. Marganski, S. Kim, C. T. Brown, V. Gunderia, M. Dembo and J. Y. Wong, *Biophys. J.*, 2003, **85**, 3329–3335.
59 J. A. Rowley and D. J. Mooney, *J. Biomed. Mater. Res.*, 2002, **60**, 217–223.
60 R. Oria, T. Wiegand, J. Escribano, A. Elosegui-Artola, J. J. Uriarte, C. Moreno-Pulido, I. Platzman, P. Delcanale, L. Albertazzi, D. Navajas, X. Trepat, J. M. García-Aznar, E. A. Cavalcanti-Adam and P. Roca-Cusachs, *Nature*, 2017, **552**, 219–224.
61 B. L. Ekerdt, R. A. Segalman and D. V. Schaffer, *Biotechnol. J.*, 2013, **8**, 1411–1423.
62 W. R. Legant, J. S. Miller, B. L. Blakely, D. M. Cohen, G. M. Genin and C. S. Chen, *Nat. Methods*, 2010, **7**, 969–971.
63 W. R. Legant, A. Pathak, M. T. Yang, V. S. Deshpande, R. M. McMeeking and C. S. Chen, *Proc. Natl. Acad. Sci. U. S. A.*, 2009, **106**, 10097–10102.
64 J. M. Viola, C. M. Porter, A. Gupta, M. Alibekova, L. S. Prahl and A. J. Hughes, *Adv. Mater.*, 2020, **2002195**, e2002195.
65 S. Khetan, M. Guvendiren, W. R. Legant, D. M. Cohen, C. S. Chen and J. A. Burdick, *Nat. Mater.*, 2013, **12**, 458–465.
66 J. N. Roberts, J. K. Sahoo, L. E. McNamara, K. V. Burgess, J. Yang, E. V. Alakpa, H. J. Anderson, J. Hay, L.-A. Turner, S. J. Yarwood, M. Zelzer, R. O. C. Ore, R. V. Ulijn and M. J. Dalby, *ACS Nano*, 2016, **10**, 6667–6679.
67 W. Li, Z. Yan, J. Ren and X. Qu, *Chem. Soc. Rev.*, 2018, **47**, 8639–8684.
68 C. Loebel, R. L. Mauck and J. A. Burdick, *Nat. Mater.*, 2019, **18**, 883–891.
69 J. Dumbleton, P. Agarwal, H. Huang, N. Hogrebe, R. Han, K. J. Gooch and X. He, *Cell. Mol. Bioeng.*, 2016, **9**, 277–288.